Converting the Liquid Electrolyte of Li Batteries into a Catalyst for CO 2 RR via Laser Irradiation

Feihong Ren, Kun Qi, Jiefeng Liu, Patrice Huguet, Damien Voiry, Stefano Deabate

Converting via laser irradiation the liquid electrolyte of Li batteries into catalyst for CO₂RR

Feihong Ren,# Kun Qi,#, Jiefeng Liu, Patrice Huguet, Damien Voiry, and Stefano Deabate **

ABSTRACT. Li-based batteries are currently the most widely used energy storage technology in electric vehicles and portable electronic devices, but discarded batteries represent a growing environmental hazard. The flammability of the liquid electrolyte particularly requires to explore alternative recycling methods. Herein, we report the photochemical conversion of usual carbonate-based electrolytes into a new catalyst with remarkable activity and selectivity for the CO_2 reduction reaction. Solutions of $LiPF_6$ in different organic solvents are first deposited on a Cu substrate and irradiated by 1.88 eV laser. After air exposure, a layer consisting of LiF and graphitic carbon deposited on Cu_xO is obtained. When tested for the electrochemical reduction of CO_2, this material converts *in situ* into an effective catalyst with a faradic efficiency as high as 46.7 % for the CH_4 and maintained above 40 % for at least 100 hours.

KEYWORDS: Li batteries, electrolyte, recycling, photochemical reaction, CO₂RR, electrocatalyst

1. INTRODUCTION. Lithium batteries have been taking a crucial role for mobility and the grid-scale energy storage.[1] This implies that the amount of discarded Li batteries entering the waste stream has increased significantly in recent years.[2,3] So, effective recycling of batteries becomes

essential to avoid environmental pollution and waste of resources. Recycling of Li batteries not only concerns the metal elements constituting the electrodes (Ni, Co, Mn, etc.) but also the electrolyte, which is often neglected.[4-6] It should then be pointed out that the current way of recycling the liquid electrolyte, which consists of separating and regenerating the different Li salts and solvents by precipitation/distillation or extraction, is complex and expensive.[7,8] Developing new methods to convert the wasted electrolyte into other useful materials could then represent an interesting, alternative solution for recycling. Here, we show for the first time how typical carbonate electrolytes can be easily converted by laser irradiation into effective catalysts for the CO_2 reduction reaction (CO_2RR).[9]

With an estimated annual emission of nearly 40 GT, carbon dioxide is one of the main greenhouse gas. Nowadays, the risks of excess CO_2 in the atmosphere are universally recognized. The electrochemical CO_2 reduction (ECR) to valuable chemicals represents a sustainable technology to achieve a carbon-neutral energy cycle in the environment when combined to carbon-free energy source.[9,10] However, the performance of ECR is hindered by the difficulty of the CO_2 activation, a poor products selectivity and the occurring of competitive hydrogen evolution. The electrochemical reduction of CO_2 requires its activation on catalyst surfaces. Research carried out so far have led to the identification that copper is one of the best catalysts for the electroreduction of CO_2 into hydrocarbons[9,11] and that selectivity can be tuned by controlling the nature of the catalyst surface and the oxidation degree of the metal.[12]

Herein, we report a new catalyst for CO_2RR with improved activity and selectivity, which can be easily obtained by the photochemical degradation of widely used carbonate electrolytes for Li batteries i.e. $LiPF_6$ in ethylene (EC) and diethyl carbonates (DEC). The electrolyte, in contact with a Cu substrate, is first irradiated by a laser source and then, exposed to air, converted into a

layer consisting of LiF and graphitic carbon deposited on Cu_xO (LiF-Cu_xO@C). This material represents then the precursor of the CO_2RR catalyst (F-Cu_xO@C) which is subsequently obtained *in situ*, by electrochemical reduction during the CO_2 electrocatalytic conversion.

2. RESULTS AND DISCUSSION. Typically, 100 mL of 1 M solution of $LiPF_6$ in EC:DEC (1:1, v/v) is dropped on a Cu foil, then sealed between two optical glasses and irradiated by a 659.55 nm (1.88 eV) laser focused by a 50x microscope at the Cu surface at a power density of 31.2 mW cm^{-2} (Figure 1a). After a few seconds, a black area can be observed. The Raman spectra collected at this location show the presence of copper oxide and carbon (Figure 1b) i.e. the CuO A_g mode at 296 cm^{-1} and the typical carbon bands at 1328 cm^{-1} and 1593 cm^{-1} corresponding to the so-called D and G modes respectively.[13,14] Accordingly, the occurring of the following reaction can be proposed:

$$Cu + carbonates \xrightarrow{\text{red laser, } LiPF_6} CuO + C \qquad (1)$$

It should be noted that dark areas can also be observed at the surface of the pristine Cu foil, due to the spontaneous oxidation at ambient conditions and/or to the manufacturing process. But Raman spectra of the as-received Cu foil (Figure S1 in SI) attest solely the presence of Cu(I) (i.e. T_{2g} and T_{1u} modes at 520 and 625 cm^{-1} respectively, belonging to the Cu_2O specie)[15] while samples obtained by photochemical reaction always contain some Cu(II) (as discussed below).

Besides the main Raman bands related to CuO and carbon, the spectrum of the material obtained by irradiation also shows weak peaks in the ranges of 710-744 cm^{-1}, 880-916 cm^{-1} and 2860-3050 cm^{-1} due to the pristine electrolyte (Figure 1b): δ C=O mode of EC at 716 cm^{-1}, C=O-Li$^+$ of EC at 730 cm^{-1}, ν P-F of PF_6^- at 741 cm^{-1}, ν C-O of EC at 893 cm^{-1}, C-O-Li$^+$ at 905 cm^{-1} and ν C-H of carbonates in the range 2860-3050 cm^{-1}.[16,17] As shown in Figure 1c, the intensity of
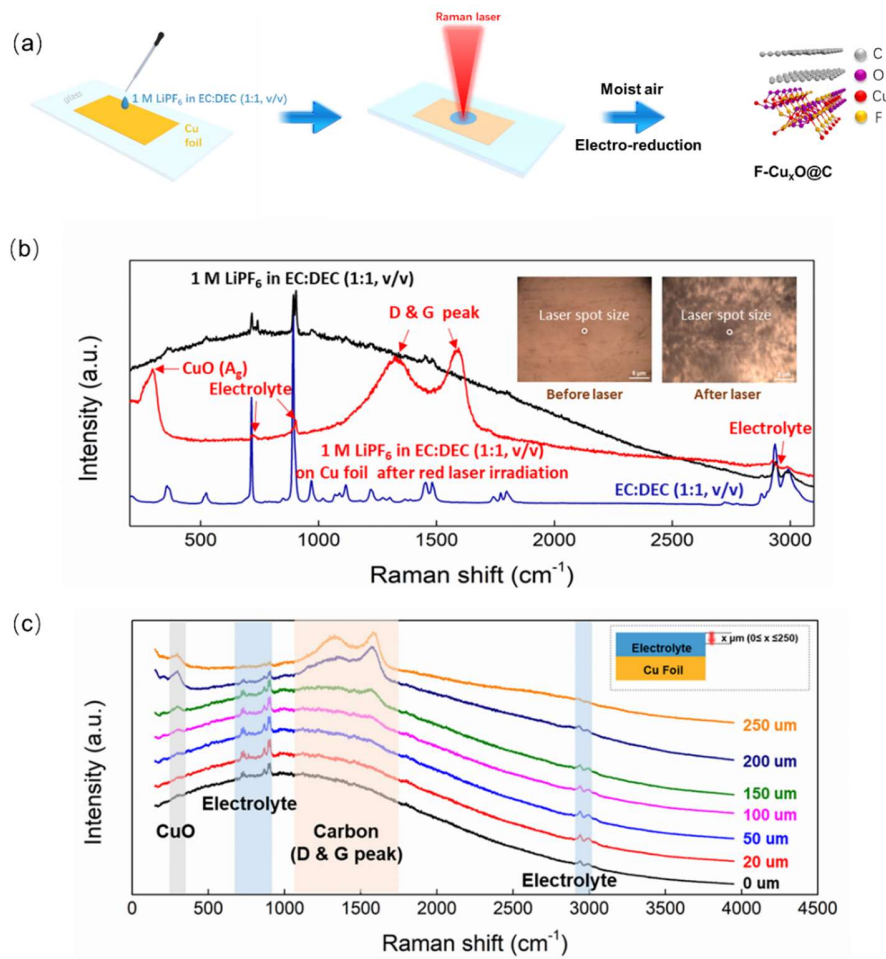
Figure 1. (a) Schematic illustration of the photochemical conversion of the electrolyte onto Cu foil. (b) Raman spectra of the conversion products from the electrolyte consisting of 1 M LiPF$_6$ in EC:DEC (1:1, v/v) irradiated at $\lambda = 659.55$ nm: comparison with spectra of the pristine electrolyte and solvent mixture alone (the insets are optical images of the Cu foil before and after irradiation). (c) Raman spectra collected at different distances from the Cu surface after the photochemical reaction: 0 μm corresponds to the starting position at the bulk electrolyte and the other values (reported in the legend) to the progressive moving of the laser focus point towards the Cu foil surface.

these peaks decreases gradually when shifting the laser focus point from the liquid electrolyte towards the Cu surface, until they cannot be detected anymore and only the bands from carbon and CuO are observed. This observation allows to confirm that the electrolyte photochemical reaction occurs at the Cu surface.

Interestingly, *in situ* Raman analysis carried out with a Li‖Cu cell shows the reversible, gradual appearance and disappearance of the D and G peaks of the carbon layer submitted to charge and discharge processes respectively (Figure S2). This behavior, previously reported by Hardwick and co-workers, can be related to the modifications induced by the Li$^+$ intercalation into the graphitic structure and the consequent loss of intensity of the ν C-C modes.[18] In short, these data show that the carbon formed by the photochemical conversion of the electrolyte is graphite-like and can participate reversibly to the electrochemical Li$^+$ intercalation/de-intercalation process.

To explore the conditions necessary for the photochemical reaction, we performed a series of experiments changing the metallic substrate, Li salt, electrolyte solvent and laser wavelength (Table 1). The corresponding Raman spectra, systematically recorded (Figure S3), show that the substrate, the laser wavelength and the presence of Li salt are the main parameters controlling the photochemical reaction, while no reaction can be observed on Al foil (Figure S3a) or with pure solvents *i.e.* without any Li salt dissolved within (Figure S3g). The absence of coordination of solvating species with the Li$^+$ cation is found to be responsible for the absence of reaction. This suggests that it is necessary to adjust the energy of ground and excited states to allow the coordinated solvent molecules to absorb the suitable energy gap and generate the intermediate reactive species necessary for the photochemical reaction.[19,20] To definitively confirm that the graphitization of the electrolyte is a photochemical process, and not just a thermal degradation

Table 1. Conditions investigated for the photochemical reaction.

Substrate	Salt	Solvent	Laser wavelength (nm)	Variate	Reaction	Figure
Cu	LiPF$_6$	EC+DEC	659.55	/	Yes	1c
Al	LiPF$_6$	EC+DEC	659.55	Substrate	No	S3a
Cu	LiPF$_6$	EC+DEC	514.58	Laser wavelength	No	S3b
Cu	LiPF$_6$	EC	659.55	Solvent	Yes	S3c
Cu	LiPF$_6$	DEC	659.55	Solvent	Yes	S3d
Cu	LiPF$_6$	DMC	659.55	Solvent	Yes	S3e
Cu	LiPF$_6$	DE	659.55	Solvent	Yes	S3f
Cu	/	EC+DEC	659.55	Salt	No	S3g
Cu	LiFSI	EC+DEC	659.55	Salt	Yes	S3h
Cu	KPF$_6$	EC+DEC	659.55	Salt	Yes	S3i

due to laser heating, we changed the laser energy to 2.42 eV (λ = 514.58) and observed no

conversion (Figure S3b).

All the different solvents studied (EC, DEC, dimethyl carbonate and diethyl ether), as well as

their mixture, can be converted into carbon by irradiation at λ = 659.55 nm if the Li salt is

dissolved within. Raman spectra collected at different depths in the experiments carried out with dimethyl carbonate (DMC) and diethyl ether (DE) based electrolytes suggest the presence of thicker carbon layers, i.e. a larger photochemical reaction rate, since weak D and G carbon peaks can be observed yet at the 0 nm position (Figures S3e and S3f). To assess the role of the salt cation or anion, we further compared the reference compound $LiPF_6$ to lithium bis(fluorosulfonyl)amide (LiFSI) and potassium hexafluorophosphate (KPF_6). Our results reveal that FSI^- and K^+ species only have a moderate influence on the photochemical reaction. Compared to $LiPF_6$, Raman spectra obtained with KPF_6 (Figure S3i) exhibit weaker D and G carbon peaks and the presence, together with the A_g mode of CuO, of the T_{2g} and T_{1u} modes of Cu_2O, suggesting a lower efficiency of the photochemical reaction. The lower reactivity observed with KPF_6 is attributed to the larger ionic diameter of K^+ compared to Li^+ and to the corresponding lower number of coordinated solvent molecules.

The composition and morphology of the layer photochemically obtained have been characterized before and after the CO_2RR electrocatalytic test. We focused our investigation on the material obtained from the 1 M $LiPF_6$ electrolyte in EC:DEC (1:1, v/v), which is the most used in commercial Li batteries. Samples have been prepared by irradiating larger surfaces of Cu (Figure S4), then exposed to air to evaporate the remaining solvent, for three different time periods: 1, 35 and 60 days. Figures 2 and 3 show X-ray photoelectron spectroscopy (XPS), scanning electron microscopy (SEM) and energy-dispersive X-ray spectroscopy (EDS) analyses of materials before the catalytic experiments. Cu 2p and Cu LMM spectra (Figures 2a and 2b respectively) indicate that the exposure time to air affects the oxidation state of the Cu substrate. Three distinct copper species are identified, corresponding to metallic Cu (918 eV), Cu_2O (916 eV) and CuO (917.6 eV).[21] The Cu/O atomic ratio calculated from the corresponding areas as
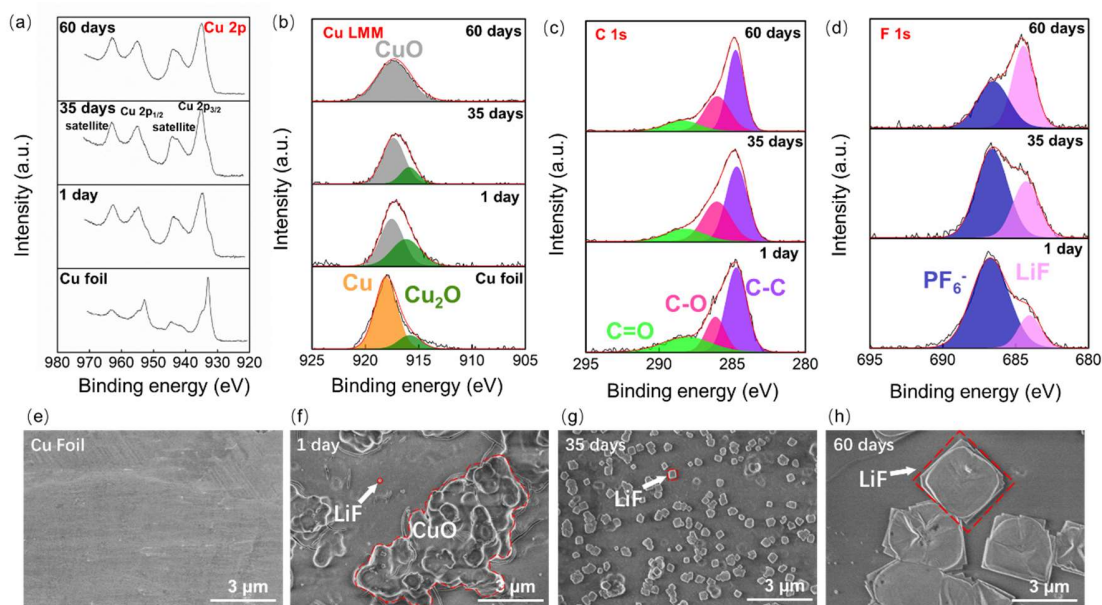
Figure 2. XPS and SEM characterization of the photochemical reaction products after different exposure times to air and comparison with the pristine Cu foil. (a) Cu 2p XPS spectra. (b) Cu LMM XPS spectra. (c) C 1s XPS spectra. (d) F 1s XPS spectra. (e) SEM image of the pristine Cu foil surface. (f) The Cu foil surface after the photochemical reaction of 1 M $LiPF_6$ in EC:DC (1:1, v/v) and 1 day exposure to air (LiF-$Cu_{1.41}$O@C). (g) After 35 days exposure (LiF-$Cu_{1.22}$O@C). (h) After 60 days exposure (LiF-CuO@C).

obtained by deconvolution of the Cu LMM spectra allows to determine the average stoichiometry of the Cu oxide. We fund that the surface oxidation degree increases with the exposition time to air. The surface composition was estimated to be $Cu_{1.41}$O, $Cu_{1.22}$O and CuO after 1, 35 and 60 exposition days respectively. The larger intensity of the satellite peaks observed in the Cu2p spectra of the irradiated samples, compared to that of the pristine Cu foil (Figure 2a), further attest the effectiveness of the photochemical treatment and exposure to the air in increasing the Cu oxidation state.[22] C 1s and F 1s spectra (Figures 2c and 2d respectively) show that the carbon phase deposited on the Cu_xO surface still contains traces of the pristine
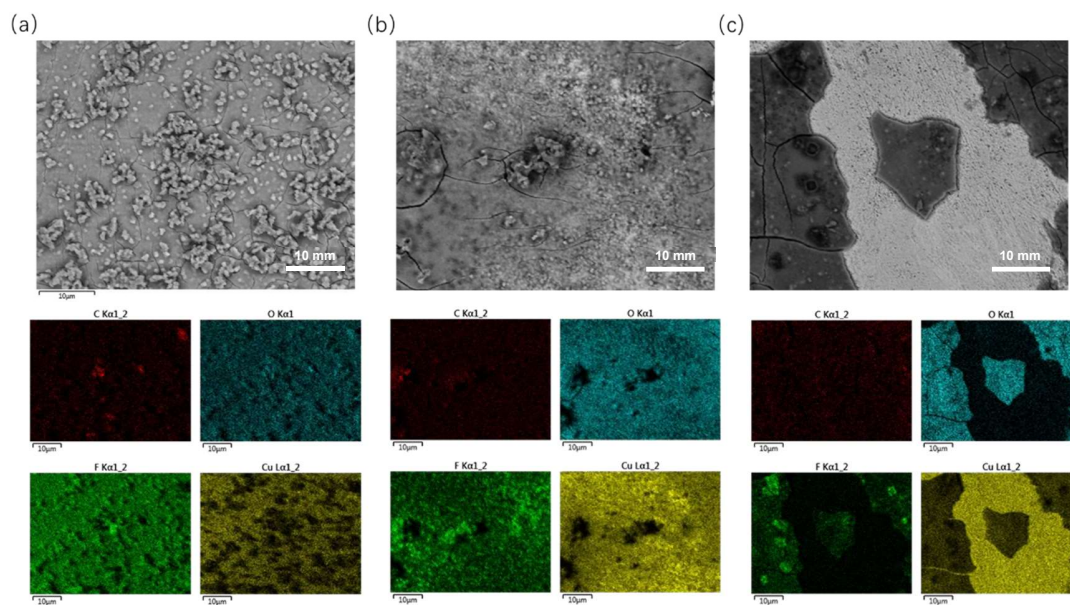
Figure 3. SEM images and corresponding EDS analysis of (a) LiF-$Cu_{1.41}O@C$, (b) LiF-$Cu_{1.22}O@C$ and (c) LiF-CuO@C.

electrolyte. C 1s spectra revealed contributions from C=O (287.8 eV), C-O (286.2 eV) and C-C (284.4 eV) bounds. The C=O signal slightly decreases with the exposure time to air while C-O and C-C increase.[23] Traces of remaining PF_6^- and LiF, are also detected at 686.8 eV and 684 eV. LiF is formed from the degradation of PF_6^- in contact with moisture in the air and the amount of LiF increases with the exposure time to air, at the expense of PF_6^-.[24] According to the previous results, the three different samples are denoted in the following as LiF-$Cu_{1.41}O@C$, LiF-$Cu_{1.22}O@C$ and LiF-CuO@C.

Results reported above are supported by the SEM and EDS analysis (Figures 2e-h and 3 respectively). The surface of the pristine Cu is largely flat (Figure 2e) while it becomes rough in the case of LiF-$Cu_{1.41}O@C$, which confirms the apparition of CuO (Figure 2f).[25] Then, increasing the exposure time corresponds to the formation of increasingly larger cubic particles

typical of crystalline LiF (Figures 2g and 2h).[26] The EDS mapping shows a relatively homogeneous distribution of the different elements analyzed for the material after one day of air exposure (Figure 3a) and the progressive transition to a more uneven surface composition with the increasing of the exposure time, according to the morphological modifications revealed by SEM (Figures 3b and 3c).

Figure 4 reports results from the SEM, EDS, XPS and extended X-ray absorption fine structure spectroscopy (EXAFS) characterizations of the material obtained after 35 days of air exposure (LiF-$Cu_{1.22}O$@C) once used for the catalysis experiments (the last consisting in linear sweep voltammetry between 0 and -1 V vs. RHE in $CO_{2(g)}$ saturated KOH solution, see below). SEM attests the disappearance of the cubic morphology characteristic of crystalline LiF (Figure 4a). At the same time, EDS analysis shows the redistribution of O, F and Cu elements according to a more uniform repartition (compare Figures 3b and 4a). XPS Cu 2p spectrum exhibits weak satellite peaks suggesting a partial reduction of the CuO phase to Cu_2O and/or Cu (Figure 4b). Interestingly, the Cu LMM and F 1s spectra show new peaks at 913.5 and 684.2 eV respectively, which can be tentatively related to the presence of a new copper oxide compound incorporating some fluoride (indicated as F-Cu_xO in the figure). This observation is supported by the EXAFS wavelet transform 2D data (Figure 4c) showing that, if only Cu-Cu bonding can be observed in the pristine Cu foil (left side), both Cu-O and Cu-F can be detected in the catalyst after the electrochemical experiments (right side). C 1s XPS spectra are similar to those obtained before the catalysis experiment. The weak decreasing of C=O species (with the corresponding increasing of C-O and C-C moieties) suggests the perpetuation of the EC and DEC decomposition during the CO_2RR experiment. Overall, our results obtained after the catalytic experiment strongly suggest that the original material LiF-Cu_xO@C obtained by
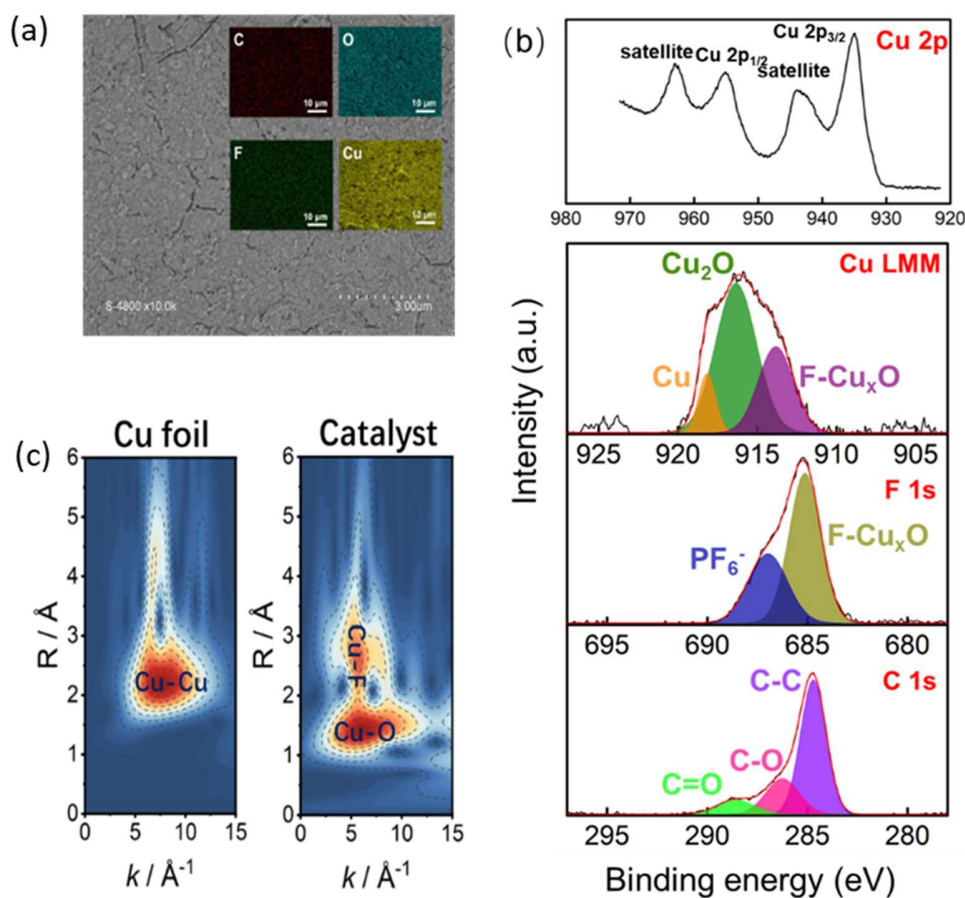
Figure 4. (a) SEM images (with the corresponding EDS mapping in the inlets), (b) XPS spectra and (c) EXAFS wavelet transform 2D plot of the photochemical reaction product LiF-$Cu_{1.22}O@C$ (exposed 35 days to air) after the catalysis experiment. EXAFS results are compared to data obtained with the pristine Cu foil (on the left side).

irradiation and exposure to the air is the precursor of the actual catalyst, consisting in a F-$Cu_xO@C$ composite which could originate from the insertion of F atoms into the Cu_xO structure. This process presumably occurs at the beginning of the electrocatalytic test *i.e.* at the onset of the potential sweep towards reduction potentials (see below).

The different materials obtained after variable exposure time to air have been investigated for the CO_2RR. The electrocatalytic experiments have been carried out with a typical gastight, two-compartment electrochemical cell using a 0.5 M KOH electrolyte saturated with CO_2 (Figure 5). Linear sweep voltammetry and chronoamperometry tests were carried out to assess the CO_2RR activity and long-term stability of the catalytic performances. Gas products were quantified by an online gas chromatograph while liquid products were collected and analysed by ^1H nuclear magnetic resonance after the tests. Electrocatalytic experiments show that the F-Cu_xO@C compounds, obtained by irradiation of the carbonate electrolyte on Cu and following exposition to the air, are able to convert CO_2 into CO, CH_4 and C_2H_4, while pristine Cu has almost no catalytic properties under the same experimental conditions. Figure 6a reports the evolution of the faradaic efficiencies (FEs) obtained for the different reaction products at -0.7 V (*vs.* the reversible hydrogen electrode, RHE) as a function of the O/Cu ratio in the as-prepared catalyst.
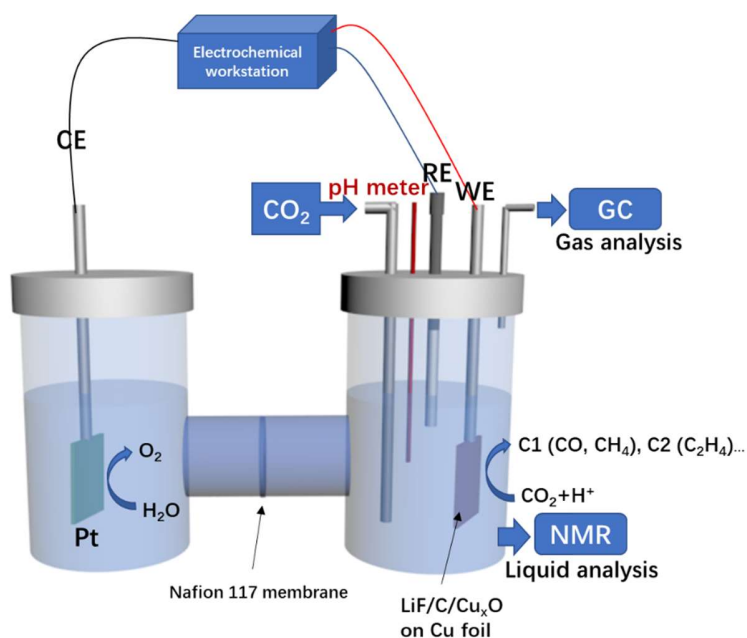

Figure 5. Experimental set-up for the CO_2RR electrochemical measurements.
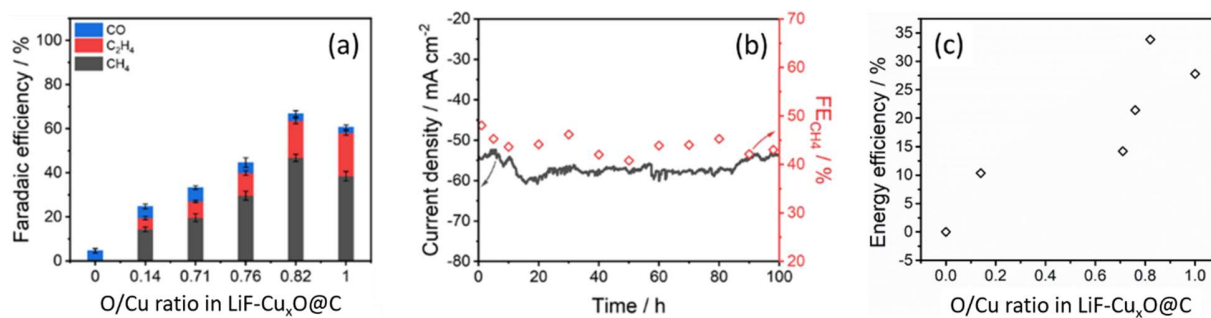
Figure 6. Results from the electrocatalytic measurements: (a) FEs as a function of the O/Cu ratio in the as-prepared catalyst, (b) long-term stability test of the catalytic activity of F-Cu$_{1.22}$O@C for the CO_2 conversion to CH_4 (V = -600 mV *vs*. RHE) and (c) energy efficiency for the CO_2 conversion to CH_4 as a function of the O/Cu ratio.

The increase of this ratio corresponds to the increase of the Cu average oxidation state. Thus, the value O/Cu = 0 corresponds to a sample of Cu foil treated with concentrated HCl to eliminate any native surface copper oxides. The value of 0.14 corresponds to the pristine Cu foil as it and the values from 0.71 to 1.00 to the LiF-Cu$_x$O@C compounds obtained by irradiation (the value of 0.71 corresponding to LiF-Cu$_{1.41}$O@C obtained after 1 day of exposure to the air and the value of 1.00 being LiF-CuO@C obtained after 60 days' exposure). The Figure S5 in SI also reports results from electrocatalytic tests carried out with a sample of pure monoxide CuO obtained by treating the pristine Cu foil with H_2O_2. Electrocatalytic measurements then show that pure Cu and CuO are just able to convert a minority part of CO_2, mainly into CO. Under the specific conditions of our experiments, the FE of pure Cu (O/Cu = 0) stays so low as 4.62 % (Figure 6a). The largest part of the FE measured with pure CuO (between the 70 and the 90 %, depending on the working potential) is due to the side reaction of $H_{2(g)}$ production (Figure S5). Typically, at -0.7 V vs RHE, the FE for H_2 was estimated to be 70.72 % compared to 24.32 %

and 0.32 % for CO and CH$_4$, respectively. Remarkably, the catalytic selectivity for the CO$_2$RR of the different LiF-Cu$_x$O@C samples is significantly larger and increases with the O/Cu ratio up to a maximum of 66.8 % for LiF-Cu$_{1.22}$O@C (O/Cu = 0.82, Figure 6a). In this case, the main product of the electrocatalytic reaction is CH$_4$ (46.72 %), followed by C$_2$H$_4$ (16.83 %) and CO (3.26 %). It is worth of noting that, when compared to other Cu based catalysts previously reported,[27-29] LiF-Cu$_{1.22}$O@C not only exhibits comparable FEs but is also relatively stable. The FE for CH$_4$ stays constant around 45 % for 100 hours with a constant current density at -55 mA cm^{-2} (Figure 6b). Finally, the partial energy efficiency calculated for the CH$_4$ production at the cathode (Figure 6c) exhibits the same trend as that of the FE and continuously increases with the Cu oxidation degree from O/Cu = 0 to 0.82. We estimated that the highest EE value for the formation of CH$_4$ is $\approx$ 34 % for LiF-Cu$_{1.22}$O@C.

3. EXPERIMENTAL SECTION.

3.1. Materials. LiPF$_6$ (98%), LiFSI (98%), KPF$_6$ (99%), KOH (90%) and KHCO$_3$ (99.7%), ethylene carbonate (98%), diethyl carbonate (99%) and dimethyl carbonate (99%) were purchased from Sigma-Aldrich Corporation. Diethyl ether (99.98%) was acquired from Fisher Scientific. All organic solvents were dehydrated before use by Sigma-Aldrich molecular sieves, 4 Å. Before use, all electrolytes were fully mixed using a minishaker MS2 IKA and, then, left for 12 h in an argon-filled glovebox (MBraun M200B, O$_2$ < 0.1 ppm and H$_2$O < 0.1 ppm). The Cu (99.9%, thickness: 8 μm) and Al foils (99%, thickness: 0.4 μm) were purchased from Goodfellow. Li foil (99.9%, thickness: 380 μm) was from Sigma-Aldrich. Nafion-117 was from Fuel Cell Store.

3.2. Synthesis of LiF-Cu$_x$O@C. 100 μL of the electrolyte was dropped on 2 x 2 cm^2 Cu foil, sealed between two glasses and irradiated by a red laser at λ = 659.55 nm during 5 h. The lighted area had

a diameter of 3.5 cm and the power density of the laser at the sample was 31.2 mW cm^{-2}. Then, the sample was exposed to air in a fuming cupboard to evaporate the remaining solvent, let H_2O traces react with Li salt to give LiF and obtain Cu surfaces at different oxidation states. Exposures for 1, 35 and 60 days correspond to obtaining the catalyst precursors LiF-Cu$_{1.41}$O@C, LiF-Cu$_{1.22}$O@C and LiF-CuO@C respectively.

3.3. Characterization. Raman spectra were recorded with a HORIBA Jobin LabRAM HR800UV confocal spectrometer (1800 grooves mm^{-1} grating, spectral resolution ~1 cm^{-1}) equipped with a charge coupled device detector (CDD) cooled by a double Peltier effect and a 50X Leica objective HCX PL Fluotar L 50X/0.55. Typically, spectra were collected with 30 s exposure time and 3 accumulations at a nominal power of 150 mW. *In situ* measurements, i.e. recorded during electrochemical operation, were carried out with the STC-Q optical cell from MTI Corporation working as a Li‖Cu electrochemical half-cell (Figure S2a) and managed by a Biologic SP-150 potentiostat. Cu and Li foils were the working and the counter electrode respectively.

SEM images were obtained with a Hitachi S4800 microscope. Elemental analysis by EDS was carried out on a Zeiss EVO HD15 device coupled with an Oxford Instruments X-Max N SDD detector.

XPS characterization was performed on a Thermo Electron ESCALAB 250 spectrometer equipped with a monochromatic radiation source (Al kα = 1486.6 eV). The analyzed surface had a diameter of 500 μm and binding energy positions were calibrated using C 1s at 284.4 eV (C-C bonding).

EXAFS spectra were obtained at the Beijing Synchrotron Radiation Facility (BSRF). Curve fitting and data analysis were carried out by the Artemis and IFEFFIT softwares. Each sample of

XAS data was aligned and processed using the Athena program. Spectra were baseline corrected using a linear pre-edge function between -200 and -50 eV and normalized using a linear or quadratic function between 150 and 700 eV, including a flattening function in the post-edge region. The XAFS signal was isolated from the adsorption edge background using a fit to a cubic spline with nodes defined by the AUTOBKG function in IFEFFIT, with a k-weight of 3 and the Rbkg parameter set to 1. Fourier transformations of k3-weighted spectra were obtained using a Kaiser-Bessel window with a 1 Å-1 sill width. The magnitude parts of the Fourier transformed spectra are reported with a radial distance scale that is not corrected for phase shift. For EXAFS fitting, theoretical scattering paths were calculated with FEFF6 using Artemis. All EXAFS spectra were fit for distances (ΔR), coordination number (CN), and mean-square displacement of interatomic distance ($\sigma 2$) using the Artemis interface with a fixed amplitude reduction factor (S_0^2) of 0.707 to 1.000. The parameters such as interatomic distance (R), CN, the difference in threshold energy (ΔE_0) and Debye-Waller factor (σ^2) were first established with reasonable guesses and then were fitted in R-space. The error in the overall fits was determined using the R-factor = $\Sigma(\chi data - \chi fit)^2 / \Sigma(\chi data)^2$. Good quality fits correspond to a R-factor < 0.05.

3.4. Electrocatalytic measurements. The study of the catalytic properties was carried out with a gastight, two-compartment electrochemical cell (Figure S5) managed by a Biologic SP-150 potentiostat. The Cu foil supporting the LiF-Cu$_x$O@C layer was the working electrode, a 3cm x 3cm platinum foil the counter electrode and the Ag/AgCl electrode was the reference. The electrolyte was 0.5 M KOH solution saturated with CO_2 at pH = 6.82 (equivalent to a 0.5 M KHCO$_3$ solution). To investigate the CO$_2$RR activity, linear sweep voltammetry was carried out from 0 to -1000 mV vs. RHE, at the 20 mV s^{-1} rate, at room temperature. A long-term stability test was also performed under chronoamperometric conditions, at a constant potential of -600 mV vs. RHE. CO$_2$RR gas

products were collected continuously during experiment and analysed every 15 min by the online gas chromatograph Micro GC-490 (Agilent) equipped with a TCD detector, a Molsieve 5A column and using Ar as carrier gas. Liquid products were collected in a cold trap and analysed by ^{1}H nuclear magnetic resonance (NMR) spectroscopy. NMR spectra of freshly acquired samples were collected on a Bruker Avance III 600 MHz spectrometer with a cryoprobe Prodigy TCI with 10 % deuterated water (D_2O) and 0.1 % (w/w) of sodium trimethylsilylpropanesulfonate as internal standard. A 1D sequence water suppression using excitation sculpting with gradients (zgesgp) was used for the acquisition (32 scans and 30s relaxation delay between pulses were used to allow complete relaxation of the protons).

The Faradaic efficiency (FE) of the CO_2 electrocatalytic conversion into gas products was calculated as following:

$$FE_{gas} = g_i \times v \times \frac{z_i}{RT} FP_0 \times \frac{1}{I_{total}} \times 100\% \qquad (1)$$

where g_i is the volume fraction of the gas product i, v the flow rate of CO_2 bubbling in the electrolyte, z_i the number of electrons required to produce one molecule of product i, I_{total} the total current, $P_0 = 1.01 \times 10^5$ Pa, T = 273.15 K, F = 96,485 C mol^{-1} and R = 8.314 J mol^{-1} K^{-1}. The FE of the CO_2 conversion into liquid products was calculated as:

$$FE_{liquid} = l_i \times \frac{z_i}{Q_{total}} F \times 100\% \qquad (2)$$

where l_i is the number of moles of liquid product i and Q_{total} is the charge passed while the liquid products are being collected. The partial energy efficiency (EE) was also calculated for the catalytic process of the CO_2 conversion into CH_4:

$$EE(\%) = \frac{\Delta E_0}{\Delta E_{applied}} \times FE \qquad\qquad\qquad (3)$$

where ΔE_0 is the equilibrium cell potential ($E_{CO2/CH4} - E_{water\ oxidation} = -0.11\ V - 1.23\ V = -1.34\ V$), $\Delta E_{applied}$ the potential applied to the cell during the experiment ($E_{CO2/CH4\ (applied)} - E_{water\ oxidation} = -0.60\ V - 1.23\ V = -1.83\ V$) and FE the Faradaic efficiency for the CO_2 conversion into CH_4 at -0.60 V vs. RHE.

4. CONCLUSIONS. This work successfully provides an original method to recycle the common electrolytes of Li-based batteries into catalyst for CO_2RR *via* laser irradiation. We identified a novel photochemical reaction for converting the carbonate electrolyte in contact with Cu and form a thin layer consisting of LiF and graphitic carbon deposited on Cu_xO. The photochemical reaction associated with the formation of the carbon layer strongly depends on the irradiation wavelength, the presence of the electrolyte and the nature of the metal substrate. This film deposited on Cu is further transformed into an effective catalyst upon electrochemical reduction under CO_2RR conditions. We have developed a facile strategy to modulate the surface oxidation degree of Cu by simply controlling the exposure time to air of the irradiated sample, which represents the easiest way to tune the selectivity of the final catalyst. We demonstrated a total FE for CO_2RR of 66.81 %, together with a robust stability of the activity for the production of CH_4 with a Faradaic efficiency around 45 % over 100 h. Taken together, our experimental results point out the key role of fluorine inserted in the Cu_xO structure for enhancing the activity and the selectivity of the catalyst and call for additional investigations at the molecular level.

ASSOCIATED CONTENT

Supporting Information. Materials, additional details on synthesis procedure, detailed experimental information on characterization techniques (Raman spectroscopy, SEM, XPS and EXAFS) and electrocatalytic measurements, additional Raman spectra of the pristine Cu foil, of the graphitic carbon obtained by photo-degradation and of the conversion products from the different irradiated electrolyte, image of the laser irradiation, scheme of the experimental set-up for the CO_2RR electrochemical measurements.

AUTHOR INFORMATION

Corresponding Authors

Damien Voiry - IEM (Institut Européen des Membranes), UMR 5635 (UM-ENSCM-CNRS), Université de Montpellier, F-34095 Montpellier, France; orcid.org/0000-0002-1664-2839; Email: damien.voiry@umontpellier.fr

Stefano Deabate - IEM (Institut Européen des Membranes), UMR 5635 (UM-ENSCM-CNRS), Université de Montpellier, F-34095 Montpellier, France; orcid.org/0000-0003-0003-0288; Email: stefano.deabate@umontpellier.fr

Authors

Feihong Ren - IEM (Institut Européen des Membranes), UMR 5635 (UM-ENSCM-CNRS), Université de Montpellier, F-34095 Montpellier, France; orcid.org/0000-0003-2390-8460

Kun Qi - IEM (Institut Européen des Membranes), UMR 5635 (UM-ENSCM-CNRS), Université de Montpellier, F-34095 Montpellier, France

Jiefeng Liu.- IEM (Institut Européen des Membranes), UMR 5635 (UM-ENSCM-CNRS), Université de Montpellier, F-34095 Montpellier, France

Patrice Huguet.- IEM (Institut Européen des Membranes), UMR 5635 (UM-ENSCM-CNRS), Université de Montpellier, F-34095 Montpellier, France

Author Contributions

#F.R. and K.Q. contributed equally to the work.

Notes

The authors declare no competing financial interest.

SUPPORTING INORMATION

Additional figures as mentioned in the text, reporting Raman spectra of the cupper foil as received; schematic of the experimental setup used for *in situ* Raman measurements and evolution of the D and G Raman peaks of the carbon layer obtained by photochemical degradation during the Li$^+$ (de-)intercalation process; Raman spectra collected for the different photochemical reaction experiments listed in Table 1; image of irradiation to obtain large-scale reaction on Cu foil; Faradaic efficiencies obtained at different potentials with the CuO sample (PDF).

REFERENCES

(1) Tarascon, J. M.; Armand, M. Issues and challenges facing rechargeable lithium batteries. *Nature* **2001**, *414*, 359–367.

(2) Winslow, K. M.; Laux, S. J.; Townsend, T. G. A review on the growing concern and potential management strategies of waste lithium-ion batteries. *Resour. Conserv. Recycl.* **2018**, *129*, 263–277.

(3) Ordonez, J.; Gago, E. J.; Girard, A. Processes and technologies for the recycling and recovery of spent lithium-ion batteries. *Renewable Sustainable Energy Rev.* **2016**, *60*, 195–205.

(4) Coman, V.; Robotin, B.; Ilea, P. Nickel recovery/removal from industrial wastes: A review. *Resour. Conserv. Recycl.* **2013**, *73*, 229–238.

(5) Fan, E. S.; Li, L.; Wang, Z. P.; Lin, J.; Huang, Y. X.; Yao, Y.; Chen, R. J.; Wu, F. Sustainable recycling technology for Li-ion batteries and beyond: challenges and future prospects. *Chem. Rev.* **2020**, *120*, 7020–7063.

(6) Huang, B.; Pan, Z. F.; Su, X. Y.; An, L. Recycling of lithium-ion batteries: Recent advances and perspectives. *J. Power Sources* **2018**, *399*, 274–286.

(7) Arshad, F.; Li, L.; Amin, K.; Fan, E.; Manurkar, N.; Ahmad, A.; Yang, J.; Wu, F.; Chen, R. A Comprehensive Review of the Advancement in Recycling the Anode and Electrolyte from Spent Lithium Ion Batteries. *ACS Sustainable Chem. Eng.* **2020**, *8*, 13527–13554.

(8) Mu, D. Y.; Liu, Z.; Jin, S.; Liu, Y. L.; Tian, S.; Dai, C. S. The Recovery and Recycling of Cathode Materials and Electrolyte from Spent Lithium Ion Batteries in Full Process. *Rog. Chem.* **2020**, *32*, 950–965.

(9) Pei, Y.; Zhong, H.; Jin, F. A brief review of electrocatalytic reduction of CO_2-Materials, reaction conditions and devices. *Energy Sci. Eng.* **2021**, *9*, 1012–1032.

(10) Zhao, Y.: Zheng, L.: Jiang, D.; Xia, W.; Xu, X.; Yamauchi, Y.; Ge, J.; Tang, J. Nanoengineering metal–organic framework-based materials for use in electrochemical CO_2 reduction reactions *Small* **2021**, *17*, 2006590.

(11) Saxena, A.; Liyanage, W.; Masud, J.; Kapila, S.; Nath, M. Selective electroreduction of CO_2 to carbon-rich products with a simple binary copper selenide electrocatalyst *J. Mater. Chem. A* **2021** *9* 7150–7161.

(12) Timoshenko, J.; Bergmann, A.; Rettenmaier, C.; Herzog, A.; Arán-Ais, R. M.; Jeon, H. S.; Haase, F. T.; Hejral, U.; Grosse, P.; Kühl, S.; Davis, E. M.; Tian, J.; Magnussen, O.; Cuenya, B.R.; Steering the structure and selectivity of CO_2 electroreduction catalysts by potential pulses *Nat. Catal.* **2022** *5* 259–267.

(13) Xu, J. F.; Ji, W.; Shen, Z. X.; Li, W. S.; Tang, S. H.; Ye, X. R.; Jia, D. Z.; Xin, X. Q. Raman spectra of CuO nanocrystals. *J. Raman Spectrosc.* **1999**, *30*, 413–415.

(14) Escribano, R.; Sloan, J. J.; Siddique, N.; Sze, N.; Dudev, T. Raman spectroscopy of carbon-containing particles. *Vib. Spectrosc.* **2001**, *26*, 179–186.

(15) Akgul, F. A.; Akgul, G.; Yildirim, N.; Unalan, H. E.; Turan, R. Influence of thermal annealing on microstructural, morphological, optical properties and surface electronic structure of copper oxide thin films. *Mater. Chem. Phys.* **2014**, *147*, 987–995.

(16) Hwang, S.; Kim, D.-H.; Shin, J. H.; Jang, J. E.; Ahn, K. H.; Lee, C.; Lee, H. Ionic conduction and solution structure in $LiPF_6$ and $LiBF_4$ propylene carbonate electrolytes. *J. Phys. Chem. C* **2018**, *122*, 19438–19446.

(17) Zhang, Y.; Zhong, Y.; Wu, Z.; Wang, B.; Liang, S.; Wang, H. Solvent molecule cooperation enhancing lithium metal battery performance at both electrodes. *Angew. Chem. Int. Ed.* **2020**, *59*, 7797–7802.

(18) Sole, C.; Drewett, N. E.; Hardwick, L. J. In situ Raman study of lithium-ion intercalation into microcrystalline graphite. *Faraday Discuss.* **2014**, *172*, 223–237.

(19) Dietzek, B.; Kiefer, W.; Hermann, G.; Popp, J.; Schmitt, M. Solvent effects on the excited-state processes of protochlorophyllide: a femtosecond time-resolved absorption study. *J. Phys. Chem. B* **2006**, *110*, 4399–4406.

(20) Moran, A. M.; Delbecque, C.; Kelley, A. M. Solvent effects on ground and excited electronic state structures of the push-pull chromophore julolidinyl-n-N,N'-diethylthiobarbituric acid. *J. Phys. Chem. A* **2001**, *105*, 10208–10219.

(21) Sung, M. M.; Kim, Y. S. Self-assembled monolayers of alkanethiols on clean copper

surfaces. *Bull. Korean Chem. Soc.* **2001**, *22*, 748–752.

(22) Wang, Y.; Lü, Y.; Zhan, W.; Xie, Z.; Kuang, Q.; Zheng, L. Synthesis of porous Cu_2O/CuO cages using Cu-based metal–organic frameworks as templates and their gas-sensing properties. J. *Mater. Chem. A* **2015**, *3*, 12796–12803.

(23) Xiao, S.; Xu, P.; Peng, Q.; Chen, J.; Huang, J.; Wang, F.; Noor, N. Layer-by-layer assembly of polyelectrolyte multilayer onto PET fabric for highly tunable dyeing with water soluble dyestuffs. *Polymers* **2017**, *9*, 735.

(24) Zheng, L.; Zhang, H.; Cheng, P.; Ma, Q.; Liu, J.; Nie, J.; Feng, W.; Zhou, Z. $Li[(FSO_2)(n-C_4F_9SO_2)N]$ versus $LiPF_6$ for graphite/$LiCoO_2$ lithium-ion cells at both room and elevated temperatures: a comprehensive understanding with chemical, electrochemical and XPS analysis. *Electrochim. Acta* **2016**, *196*, 169–188.

(25) Luan, J.; Zhang, Q.; Yuan, H.; Sun, D.; Peng, Z.; Tang, Y.; Ji, X.; Wang, H. Plasma-strengthened lithiophilicity of copper oxide nanosheet–decorated Cu foil for stable lithium metal anode. *Adv. Sci.* **2019**, *6*, 1901433.

(26) Vallejo, M. A.; Rivera, E.; Azorín, J. C.; Bernal, J.; Camacho, C.; Navarro, R.; Encarnación, E. K.; Díaz-Torres, L. A.; Sosa, M. A. Effect of Synthesis Temperature on Morphological and Luminescent Properties of Lithium Fluoride Crystals. *J. Nanosci. Nanotechnol.* **2017**, *17*, 5612–5616.

(27) Lee, S. Y.; Jung, H.; Kim, N.-K.; Oh, H.-S.; Min, B. K.; Hwang, Y. J. Mixed copper states in anodized Cu electrocatalyst for stable and selective ethylene production from CO_2 reduction. *J. Am. Chem. Soc.* **2018**, *140*, 8681–8689.

(28) Jung, H.; Lee, S. Y.; Lee, C. W.; Cho, M. K.; Won, D. H.; Kim, C.; Oh, H.-S.; Min, B. K.; Hwang, Y. J. Electrochemical fragmentation of Cu_2O nanoparticles enhancing selective C–C coupling from CO_2 reduction reaction. *J. Am. Chem. Soc.* **2019**, *141*, 4624–4633.

(29) Chou, T.-C.; Chang, C.-C.; Yu, H.-L.; Yu, W.-Y.; Dong, C.-L.; Velasco-Vélez, J.-J.; Chuang, C.-H.; Chen, L.-C.; Lee, J.-F.; Chen, J.-M. Controlling the oxidation state of the Cu electrode and reaction intermediates for electrochemical CO_2 reduction to ethylene. *J.Am. Chem. Soc.* **2020**, *142*, 2857–2867.